The Astrophysical Journal, 799:222 (11pp), 2015 February 1 doi:10.1088/0004-637X/799/2/222

SCALAR AND VECTOR NONLINEAR DECAYS OF LOW-FREQUENCY ALFVÉN WAVES

J. S. Zhao[1,2,3], Y. Voitenko[4], J. De Keyser[4], and D. J. Wu[1]
[1] Purple Mountain Observatory, Chinese Academy of Sciences, Nanjing 210008, China; js_zhao@pmo.ac.cn
[2] Key Laboratory of Solar Activity, National Astronomical Observatories, Chinese Academy of Sciences, Beijing 100012, China
[3] Key Laboratory of Modern Astronomy and Astrophysics, Nanjing University, Nanjing 210093, China
[4] Solar–Terrestrial Centre of Excellence, Space Physics Division, Belgian Institute for Space Aeronomy, Ringlaan 3 Avenue Circulaire, B-1180 Brussels, Belgium
Received 2014 August 9; accepted 2014 December 8; published 2015 January 30

ABSTRACT

We found several efficient nonlinear decays for Alfvén waves in the solar wind conditions. Depending on the wavelength, the dominant decay is controlled by the nonlinearities proportional to either scalar or vector products of wavevectors. The two-mode decays of the pump MHD Alfvén wave into co- and counter-propagating product Alfvén and slow waves are controlled by the scalar nonlinearities at long wavelengths $\rho_i^2 k_{0\perp}^2 < \omega_0/\omega_{ci}$ ($k_{0\perp}$ is wavenumber perpendicular to the background magnetic field, ω_0 is frequency of the pump Alfvén wave, ρ_i is ion gyroradius, and ω_{ci} is ion–cyclotron frequency). The scalar decays exhibit both local and nonlocal properties and can generate not only MHD-scale but also kinetic-scale Alfvén and slow waves, which can strongly accelerate spectral transport. All waves in the scalar decays propagate in the same plane, hence these decays are two-dimensional. At shorter wavelengths, $\rho_i^2 k_{0\perp}^2 > \omega_0/\omega_{ci}$, three-dimensional vector decays dominate generating out-of-plane product waves. The two-mode decays dominate from MHD up to ion scales $\rho_i k_{0\perp} \simeq 0.3$; at shorter scales the one-mode vector decays become stronger and generate only Alfvén product waves. In the solar wind the two-mode decays have high growth rates $>0.1\omega_0$ and can explain the origin of slow waves observed at kinetic scales.

Key words: magnetohydrodynamics (MHD) – plasmas – solar wind – Sun: corona – waves

1. INTRODUCTION

Alfvén waves are permeating the solar atmosphere and solar wind (e.g., Belcher & Davis 1971; Wang et al. 2012 and references therein), and their evolution is to a large extent determined by their nonlinear interactions (e.g., Hollweg 1994; Howes et al. 2008 and references therein). In the early 1960s, in the last century, it was realized that the finite-amplitude Alfvén wave is made unstable by its nonlinear coupling with another Alfvén and slow magnetoacoustic waves (Galeev & Oraevskii 1963). Namely, the initial (pump) Alfvén wave can nonlinearly decay into two product waves: the forward slow waves propagating along the background magnetic field $\mathbf{B}_0 \parallel \mathbf{z}$ in the same direction as the pump wave, and the reverse-propagating Alfvén wave. In low-β plasmas ($\beta \ll 1$) where β is the plasma/magnetic pressure ratio, the product Alfvén and slow waves have the parallel wavenumbers $-k_{0z}$ and $2k_{0z}$, respectively, with k_{0z} the parallel wavenumber of the original pump Alfvén wave. Later studies have shown that the modulation instability of Alfvén waves produces slow waves in a broad range of parallel wavenumbers (e.g., Goldstein 1978; Hollweg 1994). These theoretical predictions have been confirmed by numerous hybrid simulations (Nariyuki & Hada 2006; Araneda et al. 2008; Matteini et al. 2010; Verscharen et al. 2012; Nariyuki et al. 2012; Gao et al. 2013, 2014), which also indicated ion acceleration by the nonlinearly generated slow waves. These processes may have important implications in the solar corona and solar wind. For example, Alfvén waves driven by the solar photospheric motions and propagating outward into the interplanetary space can nonlinearly generate inward propagating Alfvén waves, initiating development of the MHD turbulence and/or reducing cross-helicity observed in the solar wind (Hollweg 1994).

In certain circumstances Alfvén waves can nonlinearly drive not only slow but also fast waves, as well as cospatial compressional fluctuations (McLaughlin et al. 2011; Thurgood & McLaughlin 2013a, 2013b). This can happen in the non-uniform solar atmosphere where the ponderomotive force can be developed by Alfvén waves due to non-zero spatial gradients of the wave amplitudes. The related nonlinear dynamics and its consequences are quite complicated, resulting in modifications of density profiles (McLaughlin et al. 2011), partial transformation into fast waves accumulating at two-dimensional (2D) null points (Thurgood & McLaughlin 2013a), and irreversible nonlinear generation of fast and slow magnetoacoustic waves that can deliver and deposit wave energy in the regions not accessible in the linear regime (Thurgood & McLaughlin 2013b).

In the recent work by Zhao et al. (2014), denoted hereafter as Paper I, the cross-scale nonlinear interactions between MHD-scale Alfvén waves and kinetic-scale Alfvén and slow waves have been investigated. It was shown that the product kinetic-scale Alfvén and slow waves can be generated by the MHD Alfvén wave through two nonlocal decay channels: the counter-propagating decay channel producing the forward slow and backward Alfvén waves, and the co-propagating decay channel producing forward slow and Alfvén waves. The former channel corresponds to the Alfvén wave decay originally considered by Galeev & Oraevskii (1963) in the MHD limit $\rho_i k_\perp \to 0$, where ρ_i is the ion gyroradius and $k_\perp$ is the wavevector component perpendicular to $\mathbf{B}_0$. The latter channel can be accessed only by taking into account kinetic effects of finite $\rho_i k_\perp$. Both channels transfer the wave energy from the large MHD scales to the small kinetic scales, similarly to the decay channels studied before (Voitenko 1998; Voitenko & Goossens 2005; Voitenko & De Keyser 2011; Zhao et al. 2011a, 2011b). In turn, the product kinetic-scale waves energize plasma particles efficiently, producing non-thermal features in the velocity distributions (Voitenko & Pierrard 2013 and references therein).

In situ solar wind measurements exhibit Alfvénic spectra extending from the MHD scales down to the kinetic scales (e.g., Sahraoui et al. 2010; He et al. 2012; Podesta 2013;

Roberts et al. 2013). If Alfvén waves are launched at large MHD scales, their nonlinear evolution to smaller scales can proceed through a turbulent cascade produced by local nonlinear interactions among counter-propagating Alfvén waves (Howes et al. 2008 and references therein), or through nonlinear decay mechanisms (Zhao et al. 2014 and references therein). The latter can produce a wide spectrum of nonlinearly generated Alfvén waves after a single step. Recent simulations have already shown such broadband distributions of nonlinearly generated Alfvén waves (Matteini et al. 2010; Verscharen et al. 2012; Gao et al. 2013). It is therefore of great interesting to investigate the role of nonlinear Alfvén decays in the turbulent cascades at different scales. But to do this, one needs first to find out what decay channel is most efficient at particular wavelength, and what are its properties.

In the present paper we extend the approach presented in Paper I by generalizing it to arbitrary perpendicular wavenumbers $\rho_i k_{0\perp}$. We show that at relatively small perpendicular wavenumber of the (pump) Alfvén wave, $\rho_i k_{0\perp} \ll \sqrt{\omega_0/\omega_{ci}}$, its two-mode decays into co- and counter-propagating Alfvén and slow waves are controlled by the scalar nonlinear interaction, whereas the vector nonlinear interaction dominates the decay at larger wavenumbers, $\rho_i k_{0\perp} \gg \sqrt{\omega_0/\omega_{ci}}$. The latter process at kinetic scales was studied by Hasegawa & Chen (1976) and Brodin et al. (2006). Here ω_0 is the pump wave frequency, ω_{ci} is the ion cyclotron frequency, and the terms "scalar" and "vector" refer to nonlinear terms proportional to the scalar $(\mathbf{k}_{0\perp}\cdot\mathbf{k}_{1\perp})$ and vector $(\mathbf{k}_{0\perp}\times\mathbf{k}_{1\perp})$ products of the pump and product wavevectors $\mathbf{k}_{0\perp}$ and $\mathbf{k}_{1\perp}$. At sufficiently short kinetic wavelengths, $\rho_i k_{0\perp}\sim 1$, the one-mode Alfvénic decay into two product Alfvén waves is strong (Erokhin et al. 1978; Volokitin & Dubinin 1989; Voitenko 1998; Zhao et al. 2010). We also discuss a competition between the one- and two-mode decays at kinetic wavelengths.

The paper is organized as follows. In Sections 2–4, we study properties of the two-mode decay. In Section 2, the basic nonlinear equations and nonlinear dispersion relations for the two-mode decay are derived; in Section 3, the nonlinear generation of the non-dissipative Alfvén and slow waves is considered; and in Section 4, the wave dissipation is accounted for. The one-mode decay and its competition with the two-mode decay are studied in Section 5. In Section 6, a general discussion is provided, including the case of broadband waves. The last section presents a summary of obtained results.

2. NONLINEAR DISPERSION EQUATIONS

A general nonlinear equation describing the nonlinear coupling among the Alfvén, fast, and slow waves is derived in Paper I in the low-frequency approximation. Let us use a local Cartesian coordinate system for every participating wave with three axes defined by the unit vectors $\hat{\mathbf{e}}_p \equiv \nabla_\perp\times\hat{\mathbf{z}}/|\nabla_\perp|$, $\hat{\mathbf{e}}_t \equiv \nabla_\perp/|\nabla_\perp|$ and $\hat{\mathbf{z}} \parallel \mathbf{B}_0$. The general nonlinear equation can be reduced to two independent nonlinear equations for the Alfvén and slow waves at $k_z^2/k_\perp^2 \ll 1$ and $m_e/m_i \ll \beta \ll 1$ (see Paper I). After comparing the orders of all nonlinear terms, we can find the dominant nonlinear effects for particular decay channels. Paper I included all the algebraic details when dealing with the nonlinear equations, and here we adopt the same routine generalizing it to arbitrary wavelength of the initial Alfvén wave.

There are three kinds of nonlinear terms in the coupling equations: the scalar terms proportional to $(\mathbf{k}_{0\perp}\cdot\mathbf{k}_{1\perp})$, the vector terms proportional to $(\mathbf{k}_{0\perp}\times\mathbf{k}_{1\perp})\cdot\hat{\mathbf{z}}$, and the nonlinear terms independent of $\mathbf{k}_{0\perp}$ and $\mathbf{k}_{1\perp}$. In what follows we will see that the scalar terms control the long-wavelength Alfvén decay, whereas the vector terms control the relatively short-wavelength decay. Quantitatively, what terms are dominant in each case depends on the relation between the normalized wavenumber $\rho^2 k_{0\perp}^2$ and frequency ω_0/ω_{ci}.

Let us first consider the wavenumber range $\rho^2 k_\perp^2 \ll \omega/\omega_{ci}$, in which case the general nonlinear equation reduces to

$$\left[\partial_t^2 - \left(1-\rho^2\partial_\perp^2\right)V_A^2\partial_z^2\right]\partial_\perp\frac{B_{pA}}{B_0} = -\omega_{ci}V_A\left(1-\rho^2\partial_\perp^2\right)\partial_z\nabla_\perp\cdot\left(\frac{n_S}{n_0}\frac{\mathbf{J}_{tA}}{J_0}\right) \quad (1)$$

for the Alfvén wave and

$$\left[\left(1-\rho^2\partial_\perp^2\right)\partial_t^2 - V_T^2\partial_z^2\right]\frac{n_S}{n_0} = -\partial_z\left[\frac{e}{m_i}(\mathbf{v}_{itA}\times\mathbf{B}_{pA})\cdot\hat{\mathbf{z}} - \mathbf{v}_{itA}\cdot\nabla_\perp v_{izA}\right] \quad (2)$$

for the slow wave. Here $-e$ is the electron charge, m_i is the ion mass, $V_T^2 = (1+T_e/T_i)V_{Ti}^2$, $V_{Ti} = \sqrt{T_i/m_i}$ is the ion thermal velocity, V_A is the Alfvén speed, T_i and T_e are the ion and electron temperatures, and $\rho = V_T/\omega_{ci}$ is the effective ion gyroradius. The plasma parameter perturbations due to the waves are n_S is the number density in slow waves, $\mathbf{B}_{pA}$ is the $\hat{\mathbf{e}}_p$-component of the Alfvén-wave magnetic field, $\mathbf{J}_{tA}$ is the $\hat{\mathbf{e}}_t$-component of the Alfvén-wave current, $\mathbf{v}_{itA}$ and v_{izA} are the ion velocity components in Alfvén waves, n_0 is the background number density and $J_0 \equiv n_0 e V_A$.

At larger wavenumbers, $\rho^2 k_\perp^2 \gg \omega/\omega_{ci}$, the nonlinear equations are

$$\left[\partial_t^2 - \left(1-\rho^2\partial_\perp^2\right)V_A^2\partial_z^2\right]\partial_\perp\frac{B_{pA}}{B_0} = \partial_z\nabla_\perp\cdot(\mathbf{v}_{ipA}\cdot\nabla_\perp\mathbf{v}_{ipS}\times\hat{\mathbf{z}} + \mathbf{v}_{ipS}\cdot\nabla_\perp\mathbf{v}_{ipA}\times\hat{\mathbf{z}}) - \frac{V_T^2}{\omega_{ci}}\partial_z\partial_\perp^2\nabla_\perp\cdot\left(\frac{n_S}{n_0}\mathbf{v}_{ipA} + \frac{n_A}{n_0}\mathbf{v}_{ipS}\right) \quad (3)$$

for the Alfvén wave and

$$\left[\left(1-\rho^2\partial_\perp^2\right)\partial_t^2 - V_T^2\partial_z^2\right]\partial_z\frac{n_S}{n_0} = -\omega_{ci}\partial_z^2\left[\left(\mathbf{v}_{ipA}\times\frac{\mathbf{B}_{pA}}{B_0}\right)\cdot\hat{\mathbf{z}} - \frac{1}{\omega_{ci}}\mathbf{v}_{ipA}\cdot\nabla_\perp v_{izA}\right] + \omega_{ci}\left(\partial_z^2 + \frac{1}{\omega_{ci}^2}\partial_\perp^2\partial_t^2\right)\left(\mathbf{v}_{epA}\times\frac{\mathbf{B}_{pA}}{B_0}\right)\cdot\hat{\mathbf{z}} \quad (4)$$

for the slow wave, where $\mathbf{v}_{ipS}$ is the $\hat{\mathbf{e}}_p$-component of the ion velocity in the slow wave, and $\mathbf{v}_{ipA}$ and $\mathbf{v}_{epA}$ are, respectively, the ion and electron velocities along $\hat{\mathbf{e}}_p$ in the Alfvén wave.

Here we consider the plane wave representation, $A = (A_k e^{-i\omega_k t + i\mathbf{k}\cdot\mathbf{r}} + c.c.)/2$, for the pump Alfvén wave $(\omega_0, \mathbf{k}_0)$, product Alfvén wave $(\omega_1, \mathbf{k}_1)$ and product slow wave $(\omega_2, \mathbf{k}_2)$. Then the wave variables in Equations (1)–(4) can be unified using the following linear responses: $\mathbf{v}_{ipS}/V_T = -i\rho k_\perp(n_S/n_0)\hat{\mathbf{e}}_p$, $\mathbf{v}_{ipA}/V_A = -(s/K)(B_{pA}/B_0)\hat{\mathbf{e}}_p$, $\mathbf{v}_{itA}/V_A = \mathbf{J}_{tA}/J_0 = i(V_A s k_z/\omega_{ci})(B_{pA}/B_0)\hat{\mathbf{e}}_t$, $\mathbf{v}_{izA}/V_A = i\sqrt{\beta}(\rho k_\perp/K^2)(B_{pA}/B_0)\hat{\mathbf{z}}$, $\mathbf{v}_{epA}/V_A = -sK(B_{pA}/B_0)\hat{\mathbf{e}}_p$, and $n_A/n_0 = i(V_A k_\perp/\omega_{ci} sK)$

(B_{pA}/B_0). Then from Equations (1)–(4), we obtain the following nonlinearly coupled dispersion equations:

$$\left(\omega_1^2 - V_A^2 k_{1z}^2 K_1^2\right)\frac{B_{1p}}{B_0} = -\frac{V_A^2 s_1 k_{1z} k_{0z} K_1^2}{2}(\hat{\mathbf{e}}_{t1}\cdot\hat{\mathbf{e}}_{t0})\frac{B_{0p}}{B_0}\frac{n_2^*}{n_0}, \tag{5}$$

$$\left(\omega_2^2 - \frac{V_T^2 k_{2z}^2}{K_2^2}\right)\frac{n_2}{n_0} = \frac{V_A^2 s_2 k_{2z} k_{0z}}{2}\frac{K_0 - s_1 K_1}{K_1^2 K_2^2 K_0}(\hat{\mathbf{e}}_{t1}\cdot\hat{\mathbf{e}}_{t0})\frac{B_{0p}}{B_0}\frac{B_{1p}^*}{B_0} \tag{6}$$

for $\rho^2 k_{0\perp}^2 \ll \omega/\omega_{ci}$, and

$$\left(\omega_1^2 - V_A^2 k_{1z}^2 K_1^2\right)\frac{B_{1p}}{B_0} = -\frac{i\omega_{ci} V_A}{2}\frac{s_1 k_{1z}}{K_0}\left(K_0^2 K_1^2 - K_2^2\right) \times (\hat{\mathbf{e}}_{t1}\times\hat{\mathbf{e}}_{t0})\cdot\hat{\mathbf{z}}\frac{B_{0p}}{B_0}\frac{n_2^*}{n_0} \tag{7}$$

$$\left(\omega_2^2 - \frac{V_T^2 k_{2z}^2}{K_2^2}\right)\frac{n_2}{n_0} = -\frac{i\omega_{ci} V_A}{2}\frac{s_2 k_{2z}}{K_0^2 K_1^2 K_2^4}\left(K_0^2 K_1^2 - K_2^2\right) \times (K_0 - s_1 K_1)(\hat{\mathbf{e}}_{t1}\times\hat{\mathbf{e}}_{t0})\cdot\hat{\mathbf{z}}\frac{B_{0p}}{B_0}\frac{B_{1p}^*}{B_0}, \tag{8}$$

for $\rho^2 k_{0\perp}^2 \gg \omega/\omega_{ci}$. Here $s_{1,2}$ indicates the propagation direction of the product waves, such that $s_{1,2} = 1$ for waves propagating along $\hat{\mathbf{z}}$, and $s_{1,2} = -1$ for waves propagating against $\hat{\mathbf{z}}$. The pump Alfvén wave is assumed propagating along $\hat{\mathbf{z}}$. The K functions describe dispersion properties of the waves, $K_0 = \sqrt{1+\rho^2 k_{0\perp}^2}$, $K_1 = \sqrt{1+\rho^2 k_{1\perp}^2}$ and $K_2 = \sqrt{1+\rho^2 k_{2\perp}^2}$. If we discard the nonlinear coupling in the right-hand sides of Equations (5)–(8), we obtain the linear dispersion relations for Alfvén and slow waves:

$$\omega_1 = V_A k_{1z} K_1, \tag{9}$$

and

$$\omega_2 = V_T k_{2z}/K_2. \tag{10}$$

The nonlinear coupling described by the right-hand sides in Equations (5)–(8) introduces nonlinear frequency shifts to ω_1 and ω_2 as well as nonlinear growth rate as shown in the Appendix. Note that we did not assume any condition for the product wavenumbers $\rho^2 k_{1\perp}^2$ and $\rho^2 k_{2\perp}^2$

3. NONLINEAR GENERATION OF NONDISSIPATIVE WAVES

To show clearly properties of the two-mode decays, we consider first a simpler case of nondissipative product waves. The corresponding nonlinear growth rate can be easily found from Equations (5)–(8) and is given by

$$\frac{\gamma_{\rm NL}^2}{\omega_0^2} \simeq -\frac{s_1 s_2}{16(\beta/2)^{1/2}}\frac{(K_0 - s_1 K_1)}{K_1 K_2 K_0^3}(\hat{\mathbf{e}}_{t1}\cdot\hat{\mathbf{e}}_{t0})^2\left|\frac{B_{0p}}{B_0}\right|^2 \tag{11}$$

at $\rho^2 k_{0\perp}^2 < \omega_0/\omega_{ci}$ and

$$\frac{\gamma_{\rm NL}^2}{\omega_{ci}^2} \simeq -\frac{s_1 s_2}{16(\beta/2)^{1/2}}\frac{1}{K_1^3 K_2^3 K_0^3}\left(K_0^2 K_1^2 - K_2^2\right)^2 \times (K_0 - s_1 K_1)\left[(\hat{\mathbf{e}}_{t1}\times\hat{\mathbf{e}}_{t0})\cdot\hat{\mathbf{z}}\right]^2\left|\frac{B_{0p}}{B_0}\right|^2 \tag{12}$$

at $\rho^2 k_{0\perp}^2 > \omega_0/\omega_{ci}$.

In the low-frequency low-wavenumber limit, $\rho^2 k_{0\perp}^2 \sim \rho^2 k_{1\perp}^2 \sim \rho^2 k_{2\perp}^2 < \omega/\omega_{ci} \ll 1$, the growth rate (11) is non-zero only for the counter-propagating product waves $s_1 = -s_2 = -1$ and reduces to the MHD growth rate found by Galeev & Oraevskii (1963). This decay is dominated by the scalar nonlinearity $\sim\hat{\mathbf{e}}_{t1}\cdot\hat{\mathbf{e}}_{t0}$, hence we will call it the scalar I decay. Besides this fully MHD local decay, there is also a nonlocal decay, $\rho k_{0\perp} \ll \rho k_{1\perp} \simeq \rho k_{2\perp}$, where the MHD Alfvén wave generates kinetic-scale Alfvén and slow waves. In this case the scalar decay rate (11) reduces to that obtained in Paper I:

$$\frac{\gamma_{\rm NL}^2}{\omega_0^2} = -\frac{s_1 s_2}{16(\beta/2)^{1/2}}\frac{(1 - s_1 K_1)}{K_1^2}(\hat{\mathbf{e}}_{t1}\cdot\hat{\mathbf{e}}_{t0})^2\left|\frac{B_{0p}}{B_0}\right|^2.$$

Note that the scalar I decay is reduced but does not vanish in this limit. Another decay, into co-propagating product waves $s_1 = s_2 = 1$, is intrinsically nonlocal; we will call it the scalar II decay.

In the wavenumber range $\rho^2 k_{0\perp}^2 > \omega_0/\omega_{ci}$ the vector nonlinear interactions and decays dominate. Equation (12) generalizes previous results by Hasegawa & Chen (1976) and Chen & Zonca (2011) on the kinetic-scale two-mode decay into Alfvén and slow product waves. From Equations (11) and (12) we find three vector decays: the counter-propagating decay into the backward Alfvén and forward slow waves ($s_1 = -s_2 = -1$, labeled as vector I decay); the co-propagating decay into forward Alfvén and slow waves ($s_1 = s_2 = 1$, vector II decay); and the counter-propagating decay with forward Alfvén and backward slow waves ($s_1 = -s_2 = 1$, vector III decay). The corresponding triplets of resonant waves in the (ω, k_z) plane are shown in Figure 1. Kinetic-scale product waves can also be generated by the channel II (see Paper I). All three channels are possible for the kinetic-scale pump Alfvén wave.

When the condition of slow nonlinear growth, $\gamma_{\rm NL} \ll \omega_{1,2}$, is violated, one needs to use the modified decay formalism (Sagdeev & Galeev 1969), and the nonlinear growth rate is consequently modified:

$$\gamma_{\rm mod} = \frac{\sqrt{3}}{2}(2\omega_2/\gamma_{\rm NL})^{1/3}\gamma_{\rm NL}. \tag{13}$$

Figures 2–4 present the nonlinear growth rates (11–13). For the comparative discussion, the growth rates are conventionally denoted as "the scalar growth rate $\gamma_{\rm NL}^s$" and "the vector growth rate $\gamma_{\rm NL}^v$", respectively. This terminology indicates what nonlinearity, scalar or vector, is dominant in each case. The same can be done for the modified decay rates (13).

Figure 2 shows $\gamma_{\rm NL}^s$ and $\gamma_{\rm NL}^v$ for the long-wavelength pump wave with $\rho_i k_{0\perp} = 10^{-4}$ in the 2D space of the wavenumber ratio $k_{1\perp}/k_{0\perp}$ and the angle θ between $\mathbf{k}_{0\perp}$ and $\mathbf{k}_{1\perp}$. It shows that the scalar growth rate is much (more than two orders) larger than the vector growth rate, which is consistent with the theoretical prediction that the scalar nonlinearities control the Alfvén wave decay at $\rho^2 k_{0\perp}^2 \ll \omega_0/\omega_{ci} = 0.01$. There are two decay channels for such waves, channels I and II. The former decay can excite the waves in the wide wavenumber range $k_{1\perp}/k_{0\perp} \sim 10^{-4}$ to 10^4, which means both local and nonlocal spectral transfer can be produced by this decay. On the contrary, the latter channel is intrinsically nonlocal and can generate only short-wavelength waves with $k_{1\perp}/k_{0\perp} \gg 1$.

Figure 3 shows $\gamma_{\rm NL}^s$ and $\gamma_{\rm NL}^v$ for the short-wavelength pump Alfvén wave with $\rho_i k_{0\perp} = 0.3$ in the 2D space of $k_{1\perp}/k_{0\perp}$ and θ. In this case the vector decay is stronger than the scalar one and its growth rate $\gamma_{\rm NL}^v$ reaches maximum at $k_{1\perp}/k_{0\perp} \sim 1$ and $\theta \sim 43^\circ$. Similar wavenumbers of all interacting waves

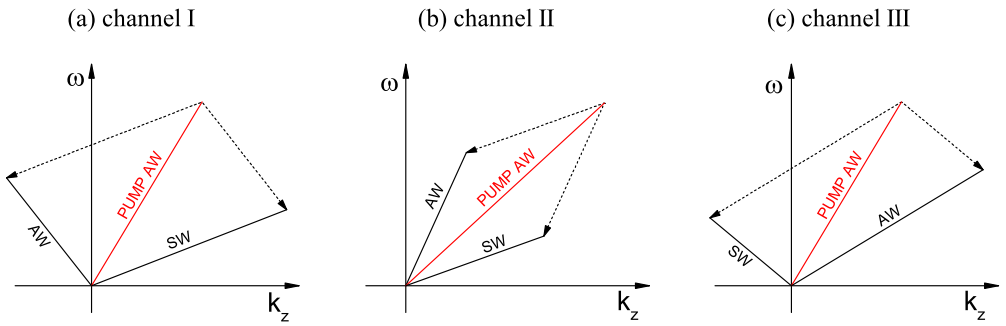

Figure 1. Three possible channels for the nonlinear decay of a pump Alfvén wave into product Alfvén and slow waves: (a) channel I, into backward Alfvén and forward slow waves; (b) channel II, into forward Alfvén and slow waves; (3) channel III, into forward Alfvén and backward slow waves. Alfvén waves are denoted as AWs and slow waves are denoted as SWs.

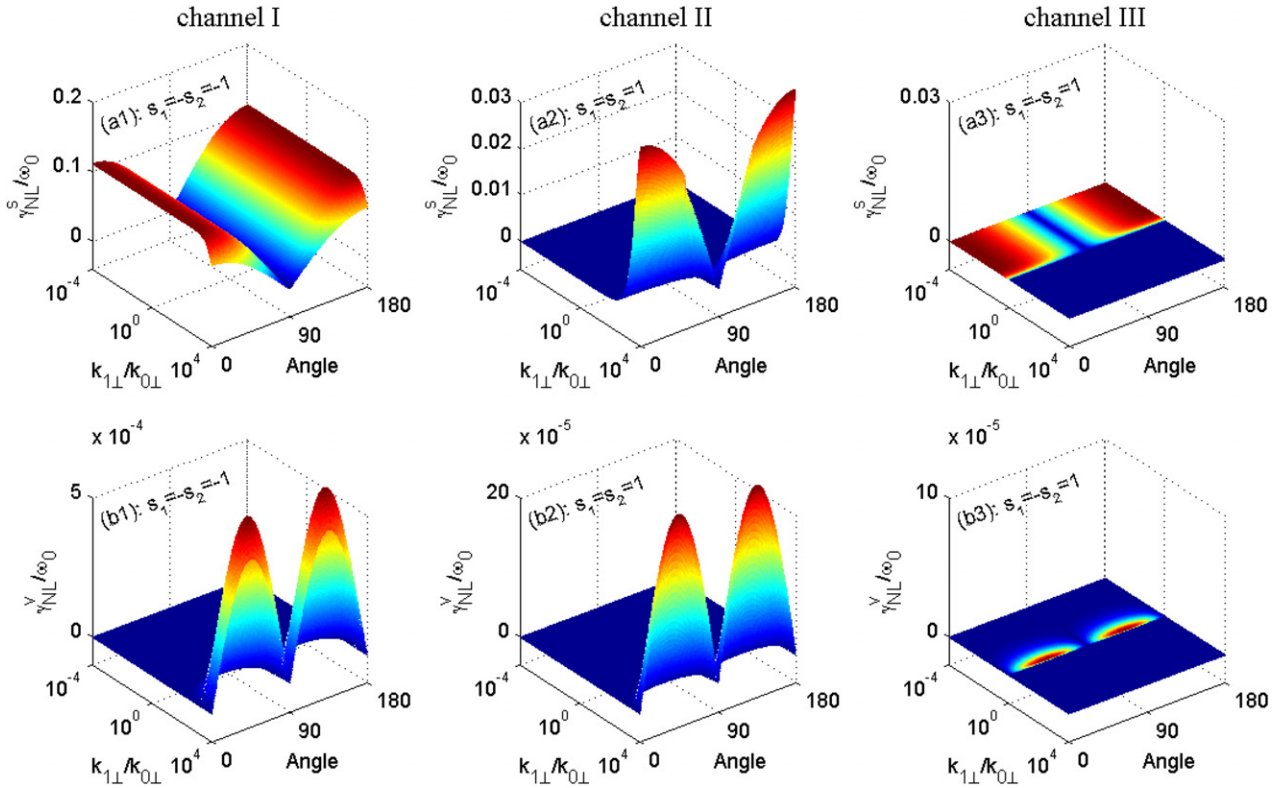

Figure 2. Scalar $\gamma^s_{\rm NL}$ (top) and vector $\gamma^v_{\rm NL}$ (bottom) nonlinear growth rates as functions of the wavenumber ratio of $k_{1\perp}/k_{0\perp}$ and the angle θ between $\hat{\mathbf{e}}_{t1}$ and $\hat{\mathbf{e}}_{t0}$ for three possible decay channels. The pump Alfvén wave is long-wavelength, $\rho_i k_{0\perp} = 10^{-4}$, the wave frequency $\omega_0/\omega_{ci} = 0.01$, and the wave amplitude $B_{0p}/B_0 = 0.1$. The ion plasma beta $\beta_i = 0.01$, the temperature ratio $T_e/T_i = 1$.

imply locality of the vector decay. Note the appearance of the channel III in Figure 3, which is still less efficient than the channels I and II.

Figure 4 shows the maximal growth rates $\gamma^s_{\rm NL}$ and $\gamma^v_{\rm NL}$ as functions of the pump wavenumber $\rho_i k_{0\perp}$ and the product/pump wavenumber ratio $k_{1\perp}/k_{0\perp}$. It again demonstrates that the scalar (vector) decay dominates at small (large) $\rho_i k_{0\perp}$.

4. NONLINEAR GENERATION OF DISSIPATIVE WAVES

In reality, the excited Alfvén and slow waves undergo Landau damping with the damping rates (see Paper I)

$$\frac{\gamma_{\rm L1}}{\Omega_1} = -\sqrt{\frac{\pi}{8}}\frac{\mu_{1i}^2}{K}\frac{T_e}{T_i}\frac{V_A}{V_{Ti}}\left[\frac{T_e}{T_i}\Lambda_0 \exp\left(-\frac{V_A^2K_1^2}{2V_{Ti}^2}\right) + \frac{V_{Ti}}{V_{Te}}\exp\left(-\frac{V_A^2K_1^2}{2V_{Ti}^2}\frac{V_{Ti}^2}{V_{Te}^2}\right)\right] \quad (14)$$

for the Alfvén wave and

$$\frac{\gamma_{\rm L2}}{\Omega_2} = 0.14 - 0.61\sqrt{\left(1+\frac{T_i}{T_e}\right)\frac{0.42+0.58\mu_{2i}^2}{0.42+0.038\mu_{2i}^2} - 1} + 0.05\left[\left(1+\frac{T_i}{T_e}\right)\frac{0.42+0.58\mu_{2i}^2}{0.42+0.038\mu_{2i}^2} - 1\right] \quad (15)$$

for the slow wave, where Ω_1 is the linear frequency of product Alfvén wave given by Equation (9), Ω_2 is the linear frequency of product slow wave given by Equation (10), $\Lambda_0 = I_0(\mu_i^2)\exp(-\mu_i^2)$, $I_0(\mu_i^2)$ is the zero-order Bessel function, and $\mu_{1,2i} \equiv \rho_i k_{1,2\perp}$. In the case of relatively slow evolution of wave amplitudes, $\gamma_{\rm L}, \gamma_{\rm NL} \ll \omega$, the growth rate of the dissipative

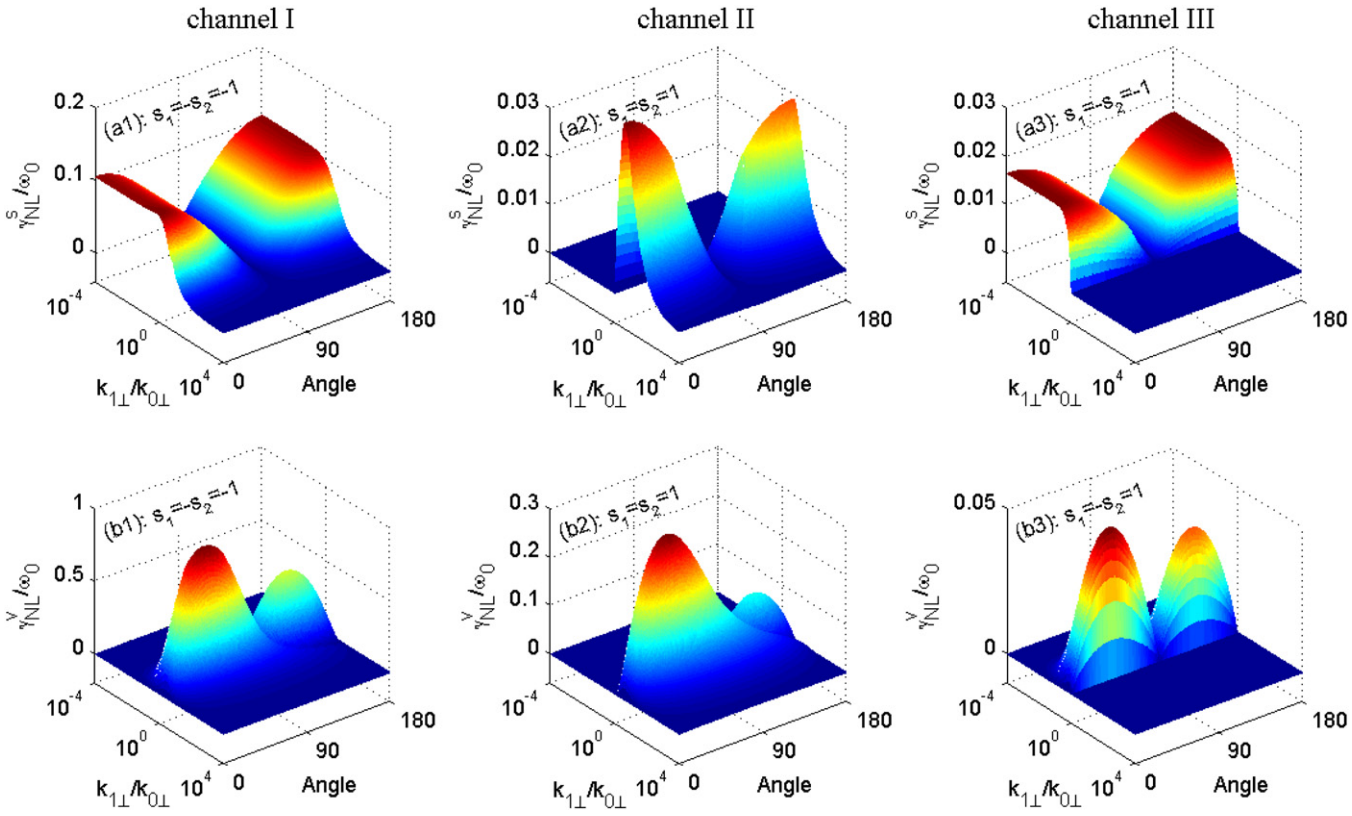

Figure 3. Scalar $\gamma_{\rm NL}^{s}$ (top) and vector $\gamma_{\rm NL}^{v}$ (bottom) nonlinear growth rates as functions of $k_{1\perp}/k_{0\perp}$ and θ for short-wavelength pump wave with $\rho_i k_{0\perp} = 0.3$, frequency $\omega_0/\omega_{ci} = 0.01$, and amplitude $B_{0p}/B_0 = 0.1$. The ion plasma beta $\beta_i = 0.01$ and temperature ratio $T_e/T_i = 1$.

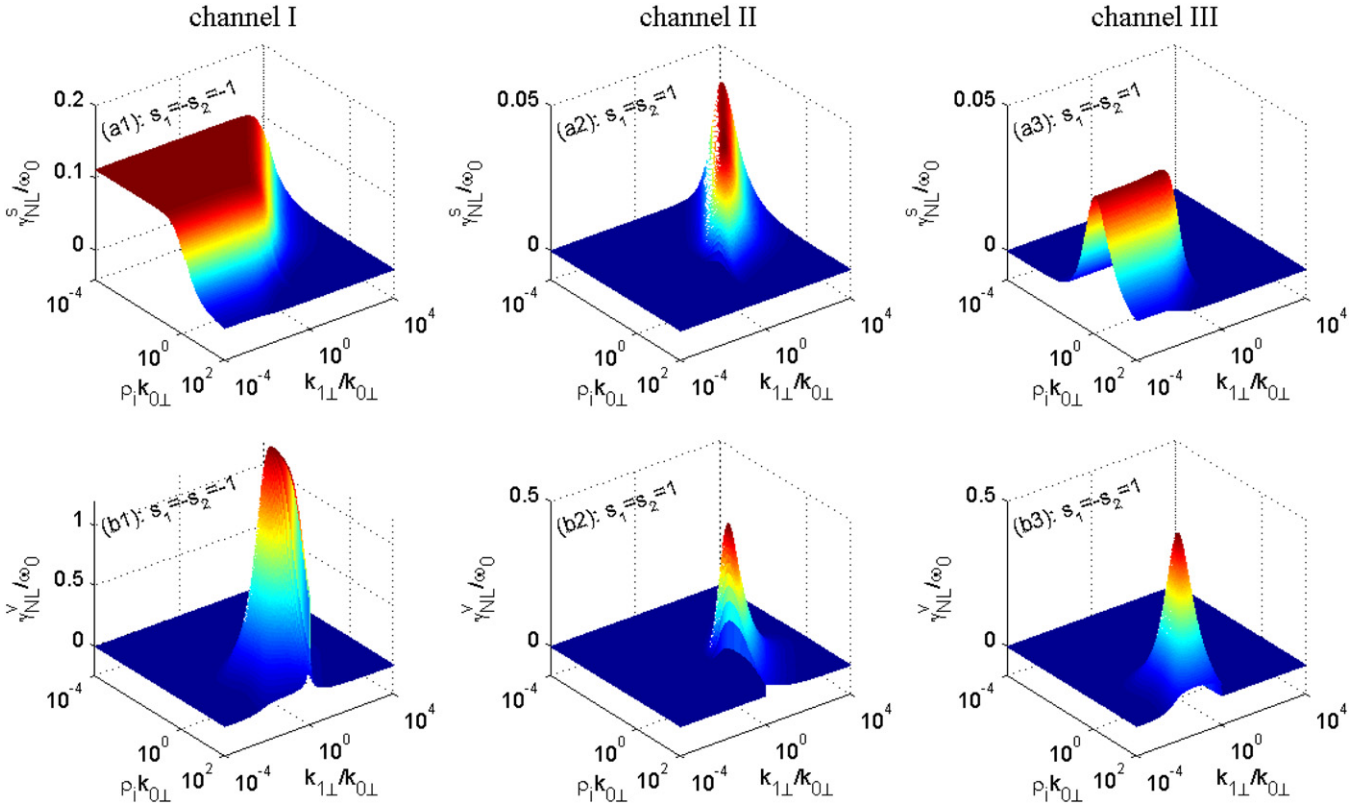

Figure 4. Maximal scalar $\gamma_{\rm NL}^{s}$ (top) and vector $\gamma_{\rm NL}^{v}$ (bottom) growth rates as functions of $\rho_i k_{0\perp}$ and $k_{1\perp}/k_{0\perp}$. The pump wave frequency $\omega_0/\omega_{ci} = 0.01$ and amplitude $B_{0p}/B_0 = 0.1$. The ion plasma beta $\beta_i = 0.01$ and temperature ratio $T_e/T_i = 1$.

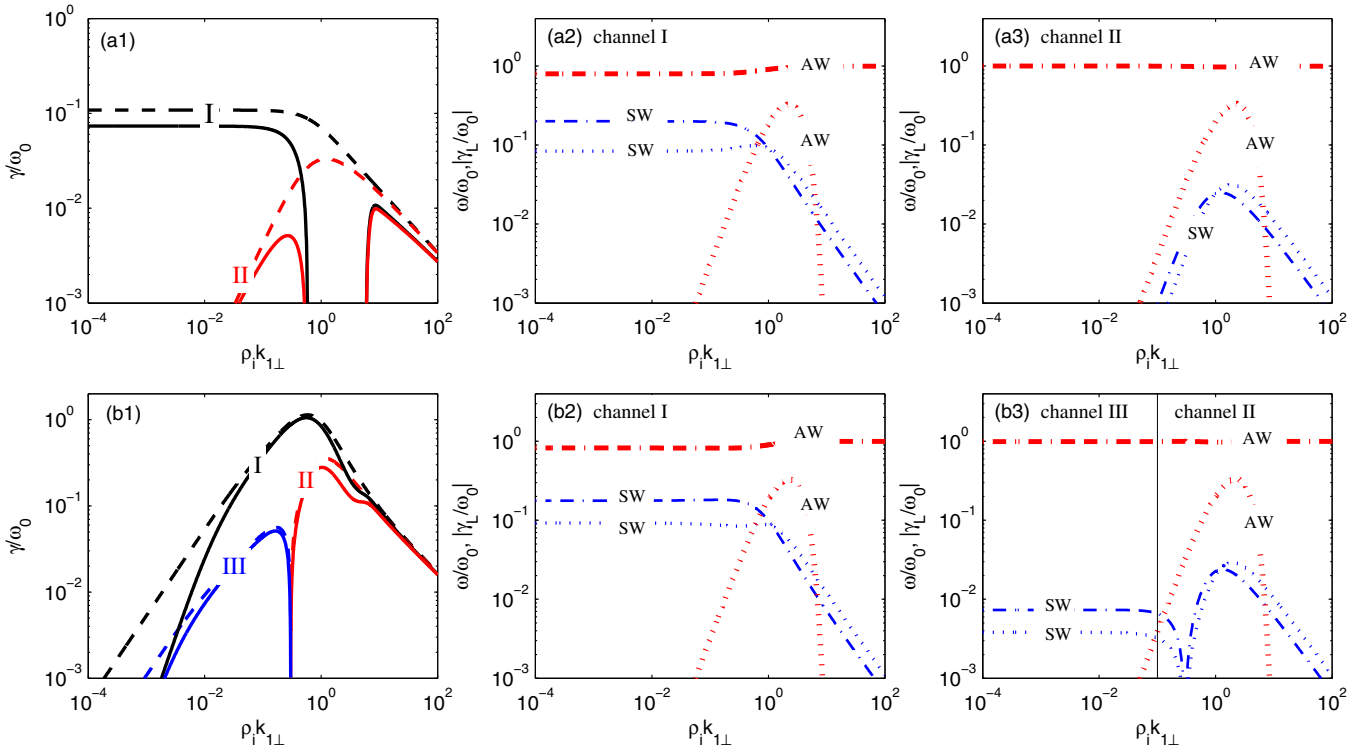

Figure 5. Nonlinear excitation rates, linear wave frequencies and Landau damping rates for the scalar (top) and vector (bottom) decays. Solid lines denote excitation rates for dissipative waves, dashed lines denote excitation rates for non-dissipative waves, dash-dotted lines denote linear wave frequencies (thick lines for Alfvén and thin lines for slow waves), and dotted lines denote Landau damping rates (thick lines for Alfvén and thin lines for slow waves). Ion plasma beta $\beta_i = 0.01$, temperature ratio $T_e/T_i = 1$, pump wave frequency $\omega_0/\omega_{ci} = 0.01$, pump wave amplitude $B_{0p}/B_0 = 0.1$, pump wavenumber $\rho_i k_{0\perp} = 0.0001$ and angle $\theta = 0^\circ$ in the scalar decay, and $\rho_i k_{0\perp} = 0.3$ and $\theta = 43^\circ$ in the vector decay.

waves is given as

$$\gamma_{\rm tot} = \frac{\gamma_{\rm L1} + \gamma_{\rm L2}}{2} \pm \sqrt{\left(\frac{\gamma_{\rm L1} - \gamma_{\rm L2}}{2}\right)^2 + \gamma_{\rm NL}^2}. \quad (16)$$

For strong nonlinear growth ($\gamma_{\rm NL} > \omega$), the growth rate can be approximately given by $\sqrt{3/4}(2\Omega_2/\gamma_{\rm tot})^{1/3}\gamma_{\rm tot}$ as was used in Paper I. Here we use a more general dispersion equation (Equation (A6) in the Appendix) to calculate the growth rate for dissipative waves. The derivation and discussion for the general dispersion equation are given in the Appendix in detail. Here we only present the result:

$$\left[x^2 - \frac{2\Omega_1}{\omega_0}\left(1 + i\frac{\gamma_{\rm L1}}{\Omega_1}\right)x + i\frac{2\Omega_1^2}{\omega_0^2}\frac{\gamma_{\rm L1}}{\Omega_1}\right] \times \left[x^2 + \frac{2\Omega_2}{\omega_0}\left(1 - i\frac{\gamma_{\rm L2}}{\Omega_2}\right)x - i\frac{2\Omega_2^2}{\omega_0^2}\frac{\gamma_{\rm L2}}{\Omega_2}\right] = \frac{4\Omega_1\Omega_2}{\omega_0^2}\frac{\gamma_{\rm NL}^2}{\omega_0^2}, \quad (17)$$

where $x \equiv (\Delta\omega + i\gamma)/\omega_0$, $\Delta\omega$ is the nonlinear frequency shift, γ is the actual growth rate, and $\gamma_{\rm NL}$ is the nonlinear driving rate (Equations (11) and (12)). We numerically solve Equation (17) in two cases, dissipative $\gamma_{\rm L1,2} \neq 0$ and non-dissipative $\gamma_{\rm L1,2} = 0$.

Figure 5 presents the resulting growth rates and frequencies of the excited waves,

$$\frac{\omega_1}{\omega_0} = 1 - s_2\sqrt{\beta/2}\frac{K_2(K_1 - s_1K_0)}{K_0K_1}; \quad (18)$$

$$\frac{\omega_2}{\omega_0} = s_2\sqrt{\beta/2}\frac{K_2(K_1 - s_1K_0)}{K_0K_1}, \quad (19)$$

restricted by the spatio-temporal resonance conditions. We see that at $\rho_i k_{1\perp} \sim 0.1$–10, where the Landau damping of Alfvén waves is strong, the nonlinear generation of dissipative waves by the scalar decay is depressed. That is why there are two separated regions where the scalar decay is efficient and can generate dissipative waves: $\rho_i k_{1\perp} \lesssim 0.1$ and $\rho_i k_{1\perp} \gtrsim 10$. On the contrary, the vector decay is stronger and hence is less affected by the Landau damping. We can also see that the nonlinear growth overcomes the linear slow wave damping at kinetic scales $\rho_i k_\perp > 1$. Note that without nonlinear pumping the (linear) damping rate of the slow wave would be larger than its frequency.

Combining all scalar and vector decays, the absolute maximum of the growth rate of dissipative waves,

$$\gamma_{\rm eff} = \max\left[\gamma_{\rm tot}^s, \gamma_{\rm tot}^v\right], \quad (20)$$

is calculated and shown in Figure 6. It is clear that (1) scalar (vector) decay dominates at long (short) wavelengths, and (2) counter-propagating decay is stronger than the co-propagating one.

From the zero-growth condition $\gamma_{\rm eff} = 0$, one usually obtains the threshold amplitude $B_{\rm thr}/B_0$ of the decay instability. Here we adopt a more realistic threshold condition of a slow growth $\gamma_{\rm eff}/\omega = 0.01$ and calculate the threshold amplitude, which is presented in Figure 8. The threshold amplitude varies in the range $B_{\rm thr}/B_0 \sim 0.01$–0.1 at $\rho_i k_{0\perp} \ll 1$. At kinetic scales, $\rho_i k_{0\perp} \sim 1$, the threshold is very low, $B_{\rm thr}/B_0 \sim 0.001$. The threshold amplitude in all cases is smaller than the wave

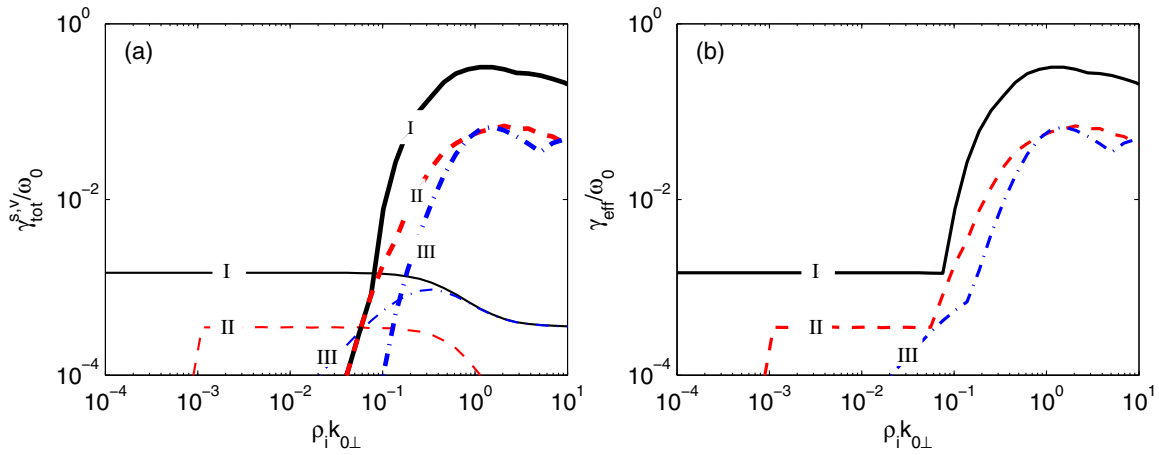

Figure 6. Nonlinear pumping rates (a), and effective excitation rate for the dissipative waves (b). Thin lines are for scalar decays and thick lines are for vector decays. Solid lines denote channel I, dashed lines denote channel II, and dash-dotted lines denote channel III. Ion plasma beta $\beta_i = 0.01$, temperature ratio $T_e/T_i = 1$, pump wave frequency $\omega_0/\omega_{ci} = 0.01$, and pump wave amplitude $B_{0p}/B_0 = 0.01$.

amplitudes observed in the solar atmosphere and solar wind, $B_{\rm obs}/B_0 \sim 0.01$–1.

The above results imply that the nonlinear decays are efficient evolution mechanisms for Alfvén waves in solar and space plasmas.

5. ONE-MODE DECAYS AND ITS COMPARISON WITH TWO-MODE DECAYS

Besides the two-mode decays generating slow and Alfvén product waves, the one-mode Alfvénic decays occur at kinetic scales. Only waves belonging to the same Alfvén wave mode participate in the one-mode decay, where the pump Alfvén wave (0) decays into two product Alfvén waves (1) and (2). The one-mode Alfvén decay has been discussed in detail by Voitenko (1998) using kinetic theory and by Voitenko & Goossens (2000) and Zhao et al. (2010) using two-fluid MHD. The one-mode decay rate is

$$\left(\frac{\gamma_{\rm NL}^{\rm one-mode}}{\omega_{ci}}\right)^2 = -\frac{1}{16\,(\beta/2)}\frac{K_1K_2}{\rho^2k_{2\perp}^2}\,(K_1 - s_1K_0)\,(K_2 - s_2K_0) \times \left(\frac{\rho^2k_{0\perp}^2}{K_0} + \frac{s_1\rho^2k_{1\perp}^2}{K_1} + \frac{s_2\rho^2k_{2\perp}^2}{K_2}\right)^2 \times |(\hat{\mathbf{e}}_{1t}\times\hat{\mathbf{e}}_{0t})\cdot\hat{z}|^2\left|\frac{B_{0p}}{B_0}\right|^2 \quad (21)$$

and the modified decay rate is

$$\gamma_{\rm mod}^{\rm onemode} = \frac{\sqrt{3}}{2}\left[2\times\min(\omega_1,\omega_2)/\gamma_{\rm NL}^{\rm onemode}\right]^{1/3}\gamma_{\rm NL}^{\rm onemode}. \quad (22)$$

There are two one-mode decays, both vectorial: decay one-mode I generating counter-propagating product waves ($s_1 = -s_2 = 1$), and decay one-mode II generating co-propagating product waves ($s_1 = s_2 = 1$). Since both product waves are Alfvénic in the one-mode decay, the decay channel III is identical to the channel I. From Equation (21) we find the decay condition $(K_1 - s_1K_0)(s_2K_0 - K_2) > 0$, which is the same as the conditions found by Voitenko (1998) and Zhao et al. (2010). This condition implies that $K_1 < K_0$ (hence $k_{1\perp} < k_{0\perp}$) in the one-mode I decay and $K_1 < K_0 < K_2$ (hence $k_{1\perp} < k_{0\perp} < k_{2\perp}$) in the one-mode II decay. Note that this decay and hence the above conditions are symmetric with respect to exchange $1 \leftrightarrows 2$. Figure 7 combines the nonlinear growth rates (21) and (22) in their validity ranges. It is seen that the growth rates reach maximum at $k_{1\perp}/k_{0\perp} \sim 1$, which implies locality of the one-mode interaction. The growth rate increases with increasing $\rho_i k_{0\perp}$, which is different from the behavior of the two-mode decay reaching an isolated maximum at the finite wavenumber $\rho_i k_{0\perp} \sim 1$ (see Figure 4).

To calculate the nonlinear excitation rate for dissipative product Alfvén waves, we use the dispersion Equation (17) with $\gamma_{\rm NL}^{\rm onemode}$ instead of $\gamma_{\rm NL}^{\rm twomode}$ and Alfvén instead of slow wave with subscript 2. A competition between the two-mode and one-mode decays is presented in Figure 8. One can see that the one-mode decay rate gradually increases with $\rho_i k_{0\perp}$ exceeding the two-mode growth rate at $\rho_i k_{0\perp} \gtrsim 0.3$. Therefore, we conclude that (1) two-mode decays dominate at MHD scales $\rho_i k_{0\perp} \ll 1$; (2) the one-mode decay dominates in the mildly/strongly dispersive range $\rho_i k_{0\perp} \geqslant 1$; and (3) both decays are important at intermediate scales, $0.1 < \rho_i k_\perp < 1$. These conclusions are also supported by the threshold amplitude shown in Panel (c). The two-mode threshold amplitude is much smaller (larger) than for the one-mode decay at $\rho_i k_{0\perp} \ll 1$ ($\rho_i k_{0\perp} \geqslant 1$). At the intermediate scales the threshold amplitudes of these decays are similar. Besides, one should note that the vector two-mode and one-mode decays do not depend on the wave frequency $\gamma/\omega_0 \propto \omega_{ci}/\omega_0$, and the decay rate of low-frequency pump wave can approach the wave frequency.

6. DISCUSSION

All two-mode and one-mode decays display anisotropic properties. Among them, scalar decays generate mainly waves propagating in the same ($\mathbf{k}_{0z}$, $\mathbf{k}_{0\perp}$) plane, and the vector decays generate primarily oblique waves out of this plane. This distinction has several important implications. First of all, scalar decays are 2D, whereas vector decays have essentially three-dimensional (3D) character. Consequently, many recent 2D simulations could not capture vector decays that are in many cases stronger. On the other hand, recent 3D hybrid simulations by Lin et al. (2012) did captured the 3D (vector) two-mode decay. Another consequence is that only vector decays can induce spectral transport across the original wavevector $\mathbf{k}_{0\perp}$ spreading the original wave spectrum in the azimuthal direction around $\mathbf{B}_0$.

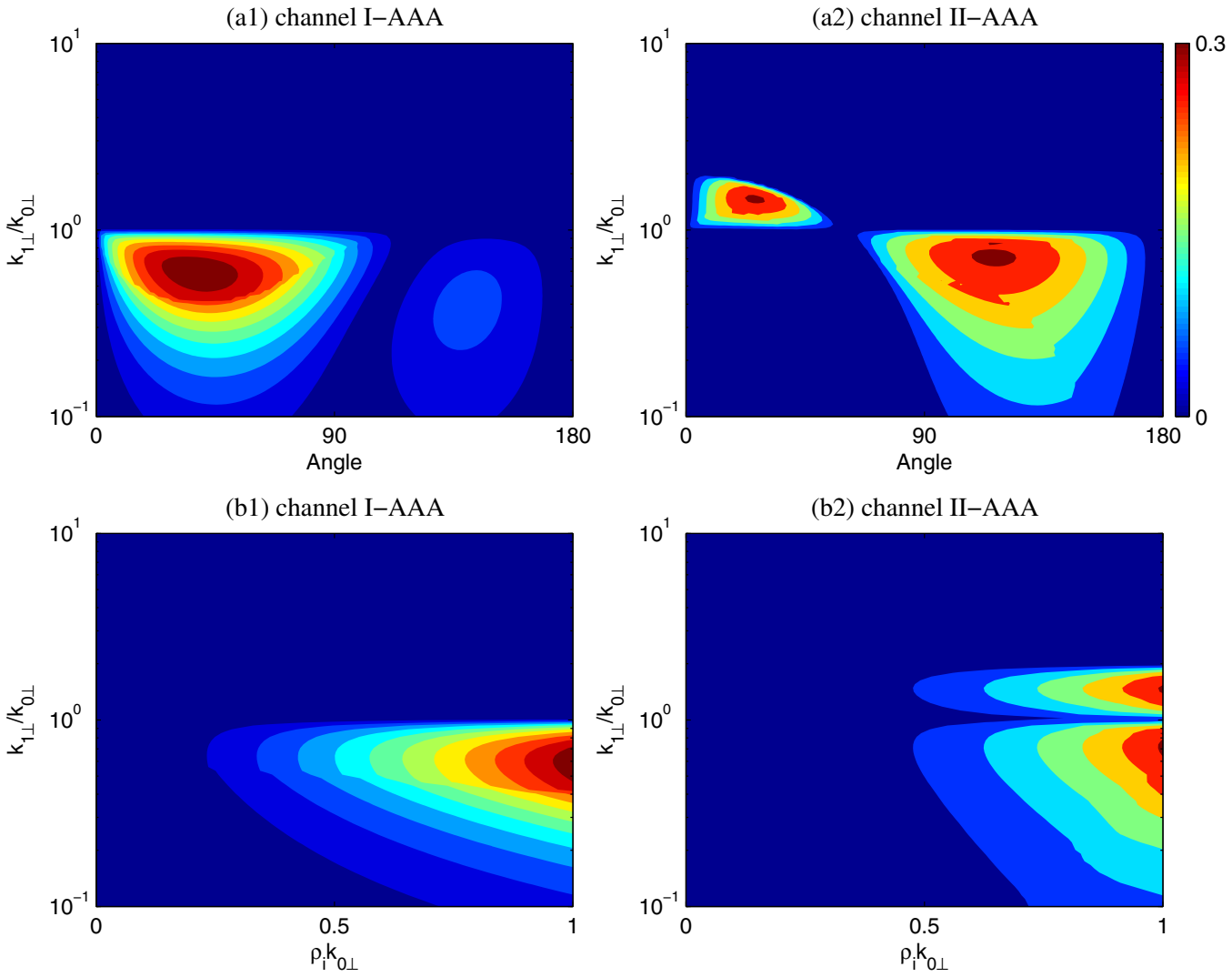

Figure 7. Nonlinear growth rates as functions of $k_{1\perp}/k_{0\perp}$ and θ (top), and nonlinear growth rates as functions of $k_{1\perp}/k_{0\perp}$ and $\rho_i k_{0\perp}$ (bottom) for the one-mode (AAA) channels I ($s_1 = -s_2 = 1$) and II ($s_1 = s_2 = 1$). Ion plasma beta $\beta_i = 0.01$, temperature ratio $T_e/T_i = 1$, pump wave frequency $\omega_0/\omega_{ci} = 0.01$, and pump wave amplitude $B_{0p}/B_0 = 0.001$. The pump wavenumber $\rho_i k_{0\perp} = 1$ is used in Panels (a1) and (a2).

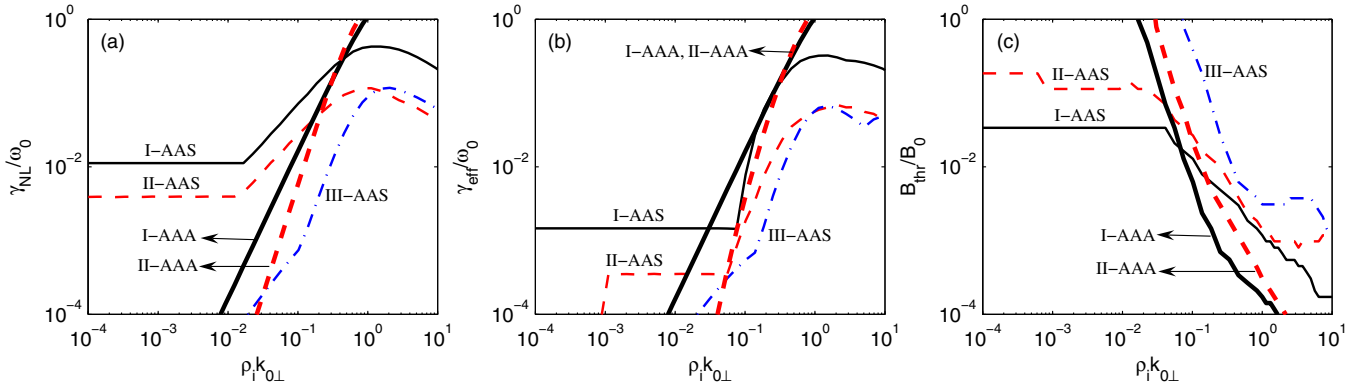

Figure 8. Comparison of the two-mode (AAS) and one-mode (AAA) decays. Growth rates of the nondissipative (a) and dissipative (b) waves, and wave threshold amplitudes (c). Ion plasma beta $\beta_i = 0.01$, temperature ratio $T_e/T_i = 1$, pump wave frequency $\omega_0/\omega_{ci} = 0.01$. Pump wave amplitude $B_{0p}/B_0 = 0.01$ in Panels (a) and (b), and threshold amplitude is found from the condition $\gamma_{\rm eff}/\omega_0 = 0.01$ in Panel (c).

It should be also noted that interaction between oblique kinetic-scale Alfvén waves and parallel slow waves propagating along $\mathbf{B}_0$, considered by Shukla & Stenflo (2000) and Sharma & Modi (2013), is weaker than the fully oblique interactions we study here. This follows from the direct comparison of the case $\mathbf{k}_{\perp 2} = 0$ in Equation (11) for parallel slow waves, and the case $\mathbf{k}_{\perp 2} \neq 0$ in Equation (12) for oblique slow waves.

The solar wind Alfvén waves usually have a broad power-law spectrum extending from the MHD to kinetic scales (e.g., Sahraoui et al. 2010; He et al. 2012; Podesta 2013;

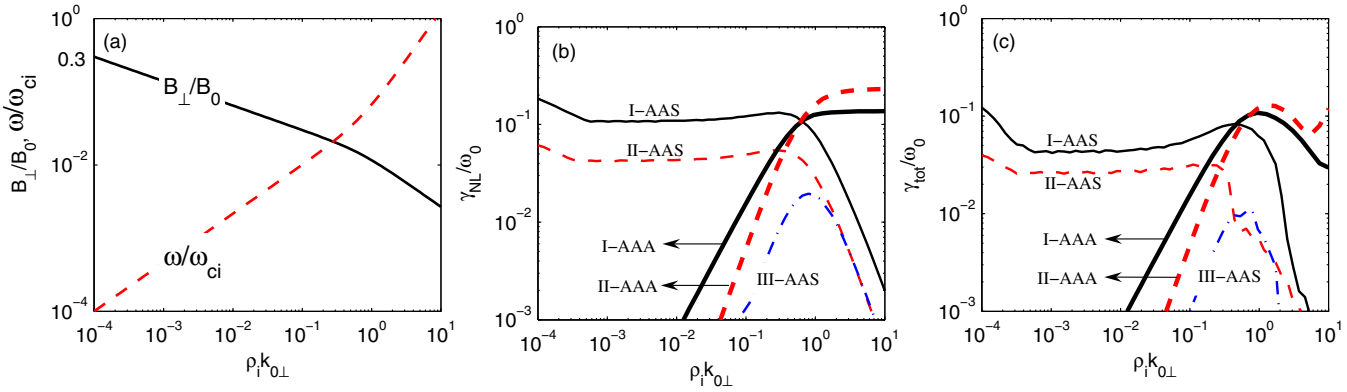

Figure 9. Amplitudes, frequencies, and nonlinear decay rates of Alfvén waves composing solar wind turbulence as functions of the perpendicular wavenumber $\rho_i k_{0\perp}$. (a) Spectrum of wave amplitudes and frequencies. Growth rates of (b) non-dissipative and (c) dissipative product waves due to one-mode (AAA) and two-mode (AAS) decays. Ion plasma beta $\beta_i = 0.1$, electron/ion temperature ratio $T_e/T_i = 1$.

Roberts et al. 2013). The MHD-range power spectrum $\sim k_\perp^{-5/3}$ is typical for the solar wind turbulence. This spectrum is thought to be produced by anisotropic turbulence cascade (e.g., Howes et al. 2008; Zhao et al. 2013 and references therein). It is interesting to estimate the obtained decay rates for individual Alfvén waves constituting this spectrum. To this end we use the following frequency and amplitude distributions of the Alfvénic fluctuations (Zhao et al. 2013):

$$\frac{\omega}{\omega_{ci}} = \left(1+\rho^2 k_\perp^2\right)^{-1/6} (k_\perp/k_{\rm ini})^{2/3}\, \frac{\omega_{\rm ini}}{\omega_{ci}}, \qquad (23)$$

and

$$\frac{B_\perp}{B_0} = \left(1+\rho^2 k_\perp^2\right)^{-1/6} (k_\perp/k_{\rm ini})^{-1/3}\, \frac{B_{\rm ini}}{B_0}, \qquad (24)$$

which results in the magnetic power spectrum $\sim(1+\rho^2 k_\perp^2)^{-1/3} k_\perp^{-5/3}$. Here $k_{\rm ini}$, $B_{\rm ini}$, and $\omega_{\rm ini}$ are the perpendicular wavenumber, magnetic field perturbation, and frequency of Alfvén waves at the turbulence driving scale.

As an example, we adopt the following parameters typical for the solar wind turbulence: $\rho_i k_{\rm ini} = 10^{-4}$, $B_{\rm ini}/B_0 = 0.3$ and $\omega_{\rm ini}/\omega_{ci} = 10^{-4}$. Using these values, in Figure 9 we plot the Alfvén wave amplitude and frequency as functions of the perpendicular wavenumber $\rho_i k_{0\perp}$ (panel (a)), and the corresponding growth rates of the decay instabilities (panels (b) and (c)). We see that the growth rates can reach values larger than 0.1ω. In general, regular Alfvénic fluctuations in the solar wind turbulence have amplitudes $B_k/B_0 = 0.1$–0.5 at MHD scales $10^{-4} < \rho_i k_\perp < 0.1$, and $B_k/B_0 \leqslant 0.1$ at kinetic scales $\rho_i k_\perp \geqslant 0.1$. We see that with these values the relative decay rates can be very high, up to $\gamma_{\rm eff}/\omega \simeq 0.3$.

Since the estimated decay rates $\gtrsim 0.1\omega$ are still lower than the cascade rate in the strong Alfvénic turbulence, $\gamma_{\rm cas} \sim \omega$ (Howes et al. 2008; Zhao et al. 2013), the strong turbulence is expected to be controlled mostly by the turbulence cascade, i.e., by the local nonlinear shearing interactions. Nevertheless, at every cascade step a fraction of energy is consumed by the two-mode decay, generating slow waves that are efficient in the ion energization (e.g., Araneda et al. 2008). Also, kinetic-scale Alfvén and slow waves are generated at almost the same rate by the nonlocal decay, which can explain kinetic slow waves observed in the solar wind (Howes et al. 2012). Since the product kinetic-scale waves are efficient in wave–particle interactions, a part of turbulent energy at large scales can avoid the inertial-range cascade and replenish the dissipation range directly, supporting energization of plasma species via dissipative product waves.

The decay-related effects should be more pronounced in the cases of weak Alfvénic turbulence, where the decay rates can be as fast as the turbulent cascade rates. Such cases need further investigations.

7. SUMMARY

We investigated nonlinear decay instabilities of Alfvén waves in a wide range from MHD to kinetic wavenumbers. Depending on the perpendicular wavenumber, the decays are controlled either by the scalar nonlinear interaction (terms proportional to the scalar product of perpendicular wave vectors, $\sim \mathbf{k}_{0\perp} \cdot \mathbf{k}_{1\perp}$), or by the vector nonlinear interaction (terms proportional to the vector product, $\sim \mathbf{k}_{0\perp} \times \mathbf{k}_{1\perp}$). In addition, the decays are differentiated by the propagation directions of product waves along or against $\mathbf{k}_{0z}$ because the decay rate depends strongly on the signs of $\mathbf{k}_{1z} \cdot \mathbf{k}_{0z}$ and $\mathbf{k}_{2z} \cdot \mathbf{k}_{0z}$. Taking into account all these important factors, we found seven decay channels, each of which can dominate in certain circumstances. The main properties of the Alfvénic decays are summarized as follows.

1. Scalar two-mode decays of the pump Alfvén wave (subscript 0) into product Alfvén (subscript 1) and slow (subscript 2) waves dominate at $\rho_i k_{0\perp} < \sqrt{\omega_0/\omega_{ci}}$, where all the interacting waves propagate in the same $(\mathbf{k}_{0z}, \mathbf{k}_{0\perp})$ plane. There are two non-negligible scalar decays: (1) scalar I decay generating counter-propagating Alfvén and co-propagating slow ($s_1 = -s_2 = -1$) product waves, and (2) scalar II decay generating only co-propagating ($s_1 = s_2 = 1$) product waves. The former decay exhibits both local and nonlocal properties, whereas the latter decay is intrinsically nonlocal. Because of their one-dimensional nature in the cross-$\mathbf{B}_0$ plane, the scalar decays do not produce an azimuthal spread of the initial Alfvénic spectrum, but can strongly accelerate cross-scale spectral transport via nonlocal nonlinear couplings. The channel III ($s_1 = -s_2 = 1$) is inefficient at long wavelengths.
2. Vector two-mode decays dominate at relatively large perpendicular wavenumbers, $\rho_i k_{0\perp} > \sqrt{\omega_0/\omega_{ci}}$, which can approach kinetic scales. These decays are strongest at $\theta \sim 43^\circ$ and are therefore 2D in the cross-$\mathbf{B}_0$ plane, producing an azimuthal spreading of the initial Alfvénic spectrum. There are three vector decays: (1) vector I decay generating counter-propagating Alfvén and co-propagating slow waves ($s_1 = -s_2 = -1$), (2) vector II decay generating only co-propagating product waves ($s_1 = s_2 = 1$),

and (3) vector III decay generating counter-propagating slow and co-propagating Alfvén waves ($s_1 = -s_2 = 1$). Among them, the vector I decay is strongest in normal circumstances.

3. In the weakly dispersive kinetic range, $0.1 < \rho_i k_{0\perp} < 1$, in addition to the two-mode vector decays, the one-mode vector decays arise generating only Alfvén product waves. All vector decays are intrinsically 3D and local; they do produce the spectral spreading in the azimuthal angle, but cannot produce the cross-scale spectral transport.
4. In the mildly/strongly dispersive range, $\rho_i k_{0\perp} \geqslant 1$, the one-mode vector decays dominate. Their growth rates reach maximum at $\theta \sim 40^\circ$ for the counter-propagating (one-mode I) decay and at $\theta \sim 25^\circ$ and 115° for the co-propagating (one-mode II) decay. Both these decays are local and 3D.
5. For the Alfvén waves composing turbulence in the solar wind, the decay rates reach high values, $\gamma_{\rm eff}/\omega_0 > 0.1$, and hence these decays are important for the wave evolution and turbulence. In particular, kinetic-scale slow modes, observed in the solar wind (Howes et al. 2012), can be generated by the local and nonlocal two-mode decays of Alfvén waves.

Combining the above results we conclude that, in general, the scalar I two-mode decay dominate at largest MHD scales $\rho_i k_{0\perp} \ll 1$, and the vector one-mode decays dominate at small kinetic scales $\rho_i k_{0\perp} \geqslant 1$. At the intermediate scales $0.1 < \rho_i k_{0\perp} < 1$ there is a competition between the two-mode vector I and the one-mode I vector decays.

The nonlinear processes studied here compete with linear generation mechanisms for kinetic Alfvén waves (Voitenko & Goossens 2003) and contribute to the kinetic-scale spectra in solar and space plasmas. The related effects and their role in particular conditions need further investigations.

This research was supported by the Belgian Federal Science Policy Office via the Solar–Terrestrial Centre of Excellence IAP Programme (project P7/08 CHARM), by the European Commission via FP7 Program (project 313038 STORM), by NSFC under grant No. 11303099, No. 11373070, and No. 41074107, by MSTC under grant No. 2011CB811402, by NSF of Jiangsu Province under grant No. BK2012495, and by Key Laboratory of Solar Activity at NAO, CAS, under grant No. KLSA201304.

APPENDIX

NONLINEAR DECAYS INTO DISSIPATIVE WAVES

Nishikawa (1968) considered the three-wave interaction by including wave dissipation. Here we use similar coupling equations as Nishikawa (1968) to study the nonlinear coupling of Alfvén and slow waves,

$$\left(\omega_1^2 - \Omega_1^2 - i2\omega_1\gamma_{D1}\right) B_{1p} = C_1 B_{0p} n_2^*, \tag{A1}$$

$$\left(\omega_2^2 - \Omega_2^2 - i2\omega_2\gamma_{D2}\right) n_2 = C_2 B_{0p} B_{1p}^*, \tag{A2}$$

where $C_{1,2}$ are the coupling coefficients, and $\Omega_{1,2}$ are the linear eigenmode frequencies, $\Omega_1 \equiv V_A k_{1z} K_1$ and $\Omega_2 \equiv V_T k_{2z}/K_2$. Equations (A1) and (A2) yield

$$\left(\omega_1^2 - \Omega_1^2 - i2\omega_1\gamma_{D1}\right)\left(\omega_2^2 - \Omega_2^2 - i2\omega_2\gamma_{D2}\right)^* = C_1 C_2^* \left|B_{0p}\right|^2. \tag{A3}$$

As the product Alfvén wave 1 is affected by the nonlinearly coupled pump wave (B_{0p}) and slow wave 2 (n_2), its frequency can be written as

$$\omega_1 = \Omega_1 + \Delta\omega + i\gamma, \tag{A4}$$

where $\Delta\omega$ and γ denote the nonlinear frequency shift and the nonlinear excitation rate. Then the slow wave frequency is given by

$$\omega_2 \simeq \Omega_2 - \Delta\omega - i\gamma, \tag{A5}$$

where the nonlinear frequency shift is ignored for the pump Alfvén wave, $\omega_0 \simeq \Omega_0$. The latter condition means that the pump wave is not much affected by the product waves. Then from Equations (A3)–(A5), we obtain the general dispersion equation

$$\left[x^2 - \frac{2\Omega_1}{\Omega_0}\left(1 + i\frac{\gamma_{L1}}{\Omega_1}\right)x + i\frac{2\Omega_1^2}{\Omega_0^2}\frac{\gamma_{L1}}{\Omega_1}\right] \times \left[x^2 + \frac{2\Omega_2}{\Omega_0}\left(1 - i\frac{\gamma_{L2}}{\Omega_2}\right)x - i\frac{2\Omega_2^2}{\Omega_0^2}\frac{\gamma_{L2}}{\Omega_2}\right] = \frac{4\Omega_1\Omega_2\gamma_{\rm NL}^2}{\Omega_0^4}, \tag{A6}$$

where $x \equiv (\Delta\omega + i\gamma)/\Omega_0$ and

$$\gamma_{\rm NL} = \sqrt{\frac{C_1 C_2^* |B_{0p}|^2}{4\Omega_1\Omega_2}}$$

is the nonlinear pumping rate.

This equation can be reduced in the following limits:

(1) weak excitation of nondissipative waves ($|x| \ll \Omega_{1,2}/\omega_0$ and $\gamma_{L1,2} = 0$),

$$x = i\frac{\gamma_{\rm NL}}{\Omega_0}; \tag{A7}$$

(2) strong excitation of nondissipative waves ($\Omega_2/\omega_0 \ll |x| \ll \Omega_1/\omega_0$ and $\gamma_{L1,2} = 0$),

$$x^3 = -\frac{2\Omega_2}{\gamma_{\rm NL}}\left(\frac{\gamma_{\rm NL}}{\Omega_0}\right)^3, \tag{A8}$$

with the unstable solution

$$x = \frac{1 + i\sqrt{3}}{2}\left(\frac{2\Omega_2}{\gamma_{\rm NL}}\right)^{1/3}\frac{\gamma_{\rm NL}}{\Omega_0}; \tag{A9}$$

(3) weak excitation of dissipative waves ($|x| \ll \Omega_{1,2}/\omega_0$ and $\gamma_{L1,2}/\Omega \ll 1$),

$$x = i\left[\frac{\gamma_{L1} + \gamma_{L2}}{2\Omega_0} + \sqrt{\left(\frac{\gamma_{L1} - \gamma_{L2}}{2\Omega_0}\right)^2 - \frac{\gamma_{\rm NL}^2}{\Omega_0^2}}\right]. \tag{A10}$$

Note that the particular expressions for the nonlinear pumping rate $\gamma_{\rm NL}$ in different decays are given by Equations (11), (12), and (21).

REFERENCES

Araneda, J. A., Marsch, E., & Vinas, A. F. 2008, PhRvL, 100, 125003
Belcher, J. W., & Davis, L. 1971, JGR, 76, 3534
Brodin, G., Stenflo, L., & Shukla, P. K. 2006, SoPh, 236, 285
Chen, L., & Zonca, F. 2011, EL, 96, 35001
Erokhin, N. S., Moiseev, S. S., & Mukhin, V. V. 1978, SvJPP, 4, 5
Galeev, A. A., & Oraevskii, V. N. 1963, SPhD, 7, 988

Gao, X. L., Lu, Q. M., Li, X., Shan, L. C., & Wang, S. 2013, PhPl, 20, 072902
Gao, X. L., Lu, Q. M., Li, X., et al. 2014, ApJ, 780, 56
Goldstein, M. L. 1978, ApJ, 219, 700
Hasegawa, A., & Chen, L. 1976, PhFl, 19, 1924
He, J. S., Tu, C. Y., Marsch, E., & Yao, S. 2012, ApJL, 745, L8
Hollweg, J. V. 1994, JGR, 99, 23431
Howes, G. G., Bale, S. D., Klein, K. G., et al. 2012, ApJL, 753, L19
Howes, G. G., Cowley, S. C., Dorland, W., et al. 2008, JGR, 113, A05103
Lin, Y., Johnson, J. R., & Wang, X. Y. 2012, PhRvL, 109, 125003
Matteini, L., Landi, S., Del Zanna, L., Velli, M., & Hellinger, P. 2010, GeoRL, 37, L20101
McLaughlin, J. A., De Moortel, I., & Hood, A. W. 2011, A&A, 527, A149
Nariyuki, Y., & Hada, T. 2006, PhPl, 13, 124501
Nariyuki, Y., Hada, T., & Tsubouchi, K. 2012, PhPl, 19, 082317
Nishikawa, K. 1968, JPSJ, 24, 916
Podesta, J. J. 2013, SoPh, 286, 529
Roberts, O. W., Li, X., & Li, B. 2013, ApJ, 769, 58
Sagdeev, R. Z., & Galeev, A. A. 1969, Nonlinear Plasma Theory (New York: Benjamin)
Sahraoui, F., Goldstein, M. L., Belmont, G., Canu, P., & Rezeau, L. 2010, PhRvL, 105, 131101
Sharma, R. P., & Modi, K. V. 2013, PhPl, 20, 082305
Shukla, P. K., & Stenflo, L. 2000, PhPl, 7, 2738
Thurgood, J. O., & McLaughlin, J. A. 2013a, SoPh, 288, 205
Thurgood, J. O., & McLaughlin, J. A. 2013b, A&A, 555, A86
Verscharen, D., Marsch, E., Motschmann, U., & Muller, J. 2012, PhRvE, 86, 027401
Voitenko, Y. 1998, JPlPh, 60, 497
Voitenko, Y., & De Keyser, J. 2011, NPGeo, 18, 587
Voitenko, Y., & Goossens, M. 2000, A&A, 357, 1073
Voitenko, Y., & Goossens, M. 2003, SSRv, 107, 387
Voitenko, Y., & Goossens, M. 2005, PhRvL, 94, 135003
Voitenko, Y., & Pierrard, V. 2013, SoPh, 288, 369
Volokitin, A. S., & Dubinin, E. M. 1989, P&SS, 37, 761
Wang, X., He, J., Tu, C., et al. 2012, ApJ, 746, 147
Zhao, J. S., Wu, D. J., & Lu, J. Y. 2010, JGR, 115, A12227
Zhao, J. S., Wu, D. J., & Lu, J. Y. 2011a, PhPl, 18, 032903
Zhao, J. S., Wu, D. J., & Lu, J. Y. 2011b, ApJ, 735, 114
Zhao, J. S., Wu, D. J., & Lu, J. Y. 2013, ApJ, 767, 109
Zhao, J. S., Voitenko, Y., Wu, D. J., & De Keyser, J. 2014, ApJ, 785, 139